Journal of Power Sources 199 (2012) 150–154

Contents lists available at SciVerse ScienceDirect

Journal of Power Sources

journal homepage: www.elsevier.com/locate/jpowsour

Short communication

$PrNi_{0.6}Co_{0.4}O_3$–$Ce_{0.8}Sm_{0.2}O_{1.9}$ composite cathodes for intermediate temperature solid oxide fuel cells

Shouguo Huang*, Qiliang Lu, Shuangjiu Feng, Guang Li, Chunchang Wang**

Laboratory of Dielectric Functional Materials, School of Physics and Materials Science, Anhui University, Hefei 230039, PR China

ARTICLE INFO

Article history:
Received 29 July 2011
Received in revised form 7 October 2011
Accepted 9 October 2011
Available online 14 October 2011

Keywords:
Solid oxide fuel cell
Cathode
Perovskite
Area specific resistance
Thermal expansion

ABSTRACT

Cobalt-containing perovskite, $PrNi_{0.6}Co_{0.4}O_3$ (PNC) has been investigated as a possible candidate for cathode material for intermediate temperature solid oxide fuel cells. It is found that the maximum and minimum electrical conductivity of PNC are 1580 S cm^{-1} at 50 °C and 1031 S cm^{-1} at 1000 °C, respectively. The thermal expansion coefficient (TEC) of the PNC is 14.21×10^{-6} K^{-1} at 700 °C. The TEC of the PNC–50 wt.% $Ce_{0.8}Sm_{0.2}O_{1.9}$ (PNC–50SDC) composite cathode is 13.49×10^{-6} K^{-1} at 700 °C, which is much more matching with the other components within the cell. The cathodic polarization of the single-phase PNC and composite cathodes with SDC shows that a weight ratio between PNC and SDC of 50:50 yields the lowest area specific resistance of 0.097 Ω cm^2 at 600 °C and 0.031 Ω cm^2 at 700 °C. The maximum power density of the PNC–50SDC cathode in an anode-supported SOFC is 1.09 W cm^{-2} at 700 °C.

1. Introduction

It is widely accepted that the performance of the solid oxide fuel cells (SOFCs) depends significantly on the cathode polarization resistance, as the operating temperature reduces to the intermediate temperature (IT) range of 600–800 °C [1,2]. $La_{0.8}Sr_{0.2}MnO_3$, as a traditional cathode using at high temperatures (800–1000 °C), is unfavorable for cathode material at intermediate temperatures since the polarization loss increases rapidly in this temperature range [3,4]. Cobalt-containing perovskites ((Ln,Sr)(Co,Fe)O_3, Ln = La, Sm, Gd, Ba and Pr) are considered as the most promising cathode materials for ITSOFCs because of their good oxygen ionic and electronic conductivities and good electrocatalytic activities towards oxygen reduction [5–14]. For instance, Shao and Haile reported that $Ba_{0.5}Sr_{0.5}Co_{0.8}Fe_{0.2}O_3$ exhibits high power densities (1010 mW cm^{-2} and 402 mW cm^{-2} at 600 °C and 500 °C, respectively) [10]. The area specific resistance of $Ba_{0.5}Sr_{0.5}Co_{0.8}Fe_{0.2}O_3$ was remarkably low: 0.055–0.071 Ω cm^2 at 600 °C, and 0.51–0.60 Ω cm^2 at 500 °C. Unfortunately, perovskites containing cobalt usually have much higher thermal expansion coefficients (TECs) ($17–24 \times 10^{-6}$ K^{-1}) than those of the electrolytes ($10–13 \times 10^{-6}$ K^{-1}) due to the electronic spin transition and particularly the thermal reduction of Co^{4+} to Co^{3+} [14].

Recently, several research groups have reported that part of the cobalt replaced by nickel in $LnCoO_3$ leads to good electrochemical performances and relative low TEC [15–19]. For example, the total conductivity of $LaNi_{0.6}Co_{0.4-y}Fe_yO_3$ is more than 500 S cm^{-1} at 1073 K, and its average thermal expansion coefficient is smaller than that of $La_{0.6}Sr_{0.4}Co_{0.2}Fe_{0.8}O_3$ (LSCF) [19]. Hjalmarsson et al. reported that the polarization resistance of the composite cathode consisting of $LaCo_{0.4}Ni_{0.6}O_3$ (LNC) and $Ce_{0.9}Gd_{0.1}O_{1.95}$ was to 0.05 ± 0.01 Ω cm^2 at 750 °C and the activation energy was be about 1 eV [15]. Therefore, the Ni-doped materials might be desirable cathode materials.

In this study, we propose $PrNi_{0.6}Co_{0.4}O_3$–$Ce_{0.8}Sm_{0.2}O_{1.9}$ (PNC–SDC) as a new cathode material. The chemical and thermal compatibilities between the cathodes and the SDC electrolytes were discussed. The cathode electrochemical performance was investigated in details.

2. Experimental

Both $PrNi_{0.6}Co_{0.4}O_3$ and $Ce_{0.8}Sm_{0.2}O_{1.9}$ powders used as cathode were prepared by glycine–nitrate process [20]. The stoichiometric amounts of Pr, Ni, and Co nitrates with analytical reagent grade were dissolved into distilled water, and then mixed with glycine to obtain a solution with pH value close to 3. The precursor solution was heated on a hot plate under stirring, leading to a viscous gel due to evaporation, and then ignited to flame, resulting in a fine "ash" with pale-black color. The "ash" was calcined at 900 °C for 4 h to remove any carbon residues remaining in the ash and finally a well-crystallined structure was obtained. Meanwhile, SDC

* Corresponding author. Tel.: +86 551 5107284; fax: +86 551 5846849.
** Corresponding author.
E-mail addresses: huangsg@ustc.edu (S. Huang), ccwang@ahu.edu.cn (C. Wang).

0378-7753/$ – see front matter © 2011 Elsevier B.V. All rights reserved.
doi:10.1016/j.jpowsour.2011.10.025

powders used as electrolyte were synthesized by using an oxalate co-precipitation method as described elsewhere [21]. The SDC powders were pressed into pellets and sintered at 1400 °C for 5 h as electrolyte substrates.

The PNC and PNC–SDC cathode powders were mixed with 3 wt.% polyvinyl buteral-76 binder, and 25 wt.% sodium-free corn oil, respectively. Methyl ethyl ketone was used as the solvent. The cathode slurries were screen-printed onto both sides of the SDC electrolyte pellets, and subsequently sintered in air at 950 °C for 2 h.

X-ray diffraction (XRD) (MXP18AHF, MARK, Japan) was used to identify the crystal structure of the prepared PNC powder and the phase reaction. The crossing-sectional images of the interfaces between electrodes and electrolyte were characterized by a scanning electron microscope (SEM, S-4800, Hitachi). The total conductivity of the well-sintered samples was measured with a standard dc four-probe technique. The pressed and sintered rectangular-shaped bars in size of 3 mm × 5 mm × 12 mm were painted with platinum paste and wired with platinum threads at both ends. The resistance was measured with a HP 34401 multimeter. The applied currents were varied between −50 and 50 mA. The distance between potential probes was 8 mm. The total conductivity was performed at temperatures ranging from 50 °C to 1000 °C in air. The total conductivity was calculated from the IV characteristics.

The samples for thermal expansion coefficient (TEC) measurements were sintered at 1100 °C for 12 h in air. Typical specimen geometry of the samples was a column-like pillar in size of Φ6 mm × 18 mm. The TEC was measured with a dilatometer (PCY-III, Xiangtan Huafeng Indus. Co.) from 25 °C to 1000 °C with a heating rate of 3 °C min^{-1} in air.

Electrochemical impedance spectroscopy (EIS) measurements were carried out with an electrochemical workstation (CHI650D, Chenhua Indus., Shanghai) in the temperature range of 500–750 °C in air. The frequency range was 0.01–10^5 Hz with a signal amplitude of 10 mV under open circuit voltage condition. Data of the impedance spectra were treated with the software Zview to obtain an equivalent circuit model.

The performance of the cathodes was evaluated in an anode-supported fuel cell. NiO–SDC (with a weight ratio of 60:40) mixture was used as the anode and SDC was used as the electrolyte. The NiO–SDC anode substrate and the SDC electrolyte film with an YSZ buffer interlayer were prepared via tape casting and co-firing process [22,23]. The electrolyte layer and anode support were co-fired at 1400 °C for 5 h, which resulted in a dense SDC film on the NiO–SDC substrate. Finally, PNC and PNC–SDC cathode slurries were subsequently screen printed onto the side of the SDC film and sintered at 950 °C for 2 h. The single-cell performance was tested at 700 °C with humidified (3% H_2O) hydrogen as the fuel and ambient air as the oxidant.

3. Results and discussion

Fig. 1 shows the XRD patterns of the PNC powder fired at 900 °C for 2 h and the PNC–SDC mixture (with a weight ratio of 50:50, PNC–50SDC) fired at 1000 °C for 24 h. It is found that the PNC oxide is of a cubic perovskite structure (space group Pm-3 m) (shown in Fig. 1a). To evaluate the phase reaction between PNC and SDC, the chemical compatibility of PNC and SDC was investigated via XRD pattern. The XRD peaks of the PNC–SDC mixture powder (shown in Fig. 1b) are ascribed to be the perovskite phase of PNC and the cubic phase of SDC. No unexpected diffraction peaks and any peak shifting are observed, indicating that PNC is chemically compatible with the SDC electrolyte under the SOFC operating condition.

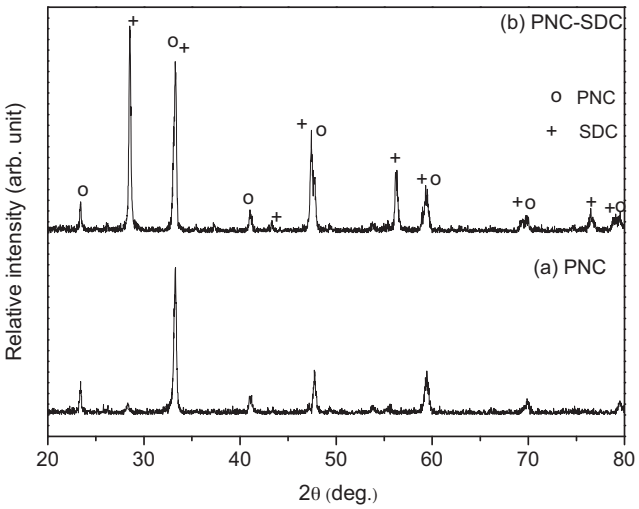

Fig. 1. X-ray diffraction patterns of (a) $PrNi_{0.6}Co_{0.4}O_3$ fired at 900 °C for 4 h and (b) $PrNi_{0.6}Co_{0.4}O_3$–$Ce_{0.8}Sm_{0.2}O_{1.9}$ mixture fired at 1000 °C for 24 h.

Fig. 2 plots the electrical conductivity of PNC from 50 °C to 1000 °C in air. The conductivity exhibits a metallic nature, which linearly decreases from 1580 S cm^{-1} at 50 °C to 1031 S cm^{-1} at 1000 °C. This metallic-like conductivity is characteristic of Co-based perovskites due to the energy band overlap between Co-3d and O-2p. These conductivity values of PNC are higher than those of LSCF in the same temperature range between 323 and 1323 K, and reach the same magnitude as those reported in LNC [6,15]. This result suggests that the PNC is a good conductor suitable for a SOFC cathode material.

Fig. 3 shows the area specific resistances (ASRs) of the PNC and PNC–SDC cathodes at various temperatures. The ASR values were deduced from the EIS defined as the difference between the low-frequency and the high-frequency intercepts with the real axis. The ASR value of the PNC cathode is 0.27 Ω cm^2 at 700 °C, which is lower than that of $LaNi_{0.6}Co_{0.4}O_3$ at the same temperature [15]. However, the ASR value of the PNC cathode is still slightly higher than the expected value of 0.15 Ω cm^2 at 700 °C.

To improve the electrochemical performance, various contents of SDC were added into the PNC. The addition of SDC into PNC causes a remarkable decrease in the interfacial polarization resistance. In the beginning range, the addition of SDC causes an obvious decrease in ASR. Then, the ASR decreases gently with further addition of SDC. For example, the area specific resistance value at 700 °C decreases

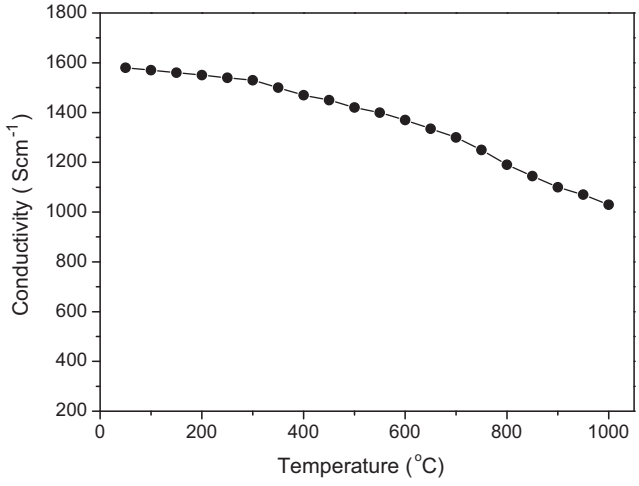

Fig. 2. Electrical conductivity of the PNC with respect to the temperature.

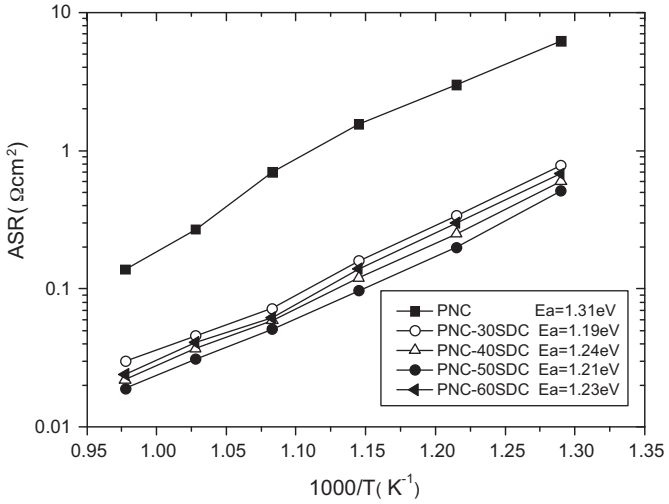

Fig. 3. Temperature-dependent area specific resistance of the PNC and PNC–SDC cathodes with different SDC contents.

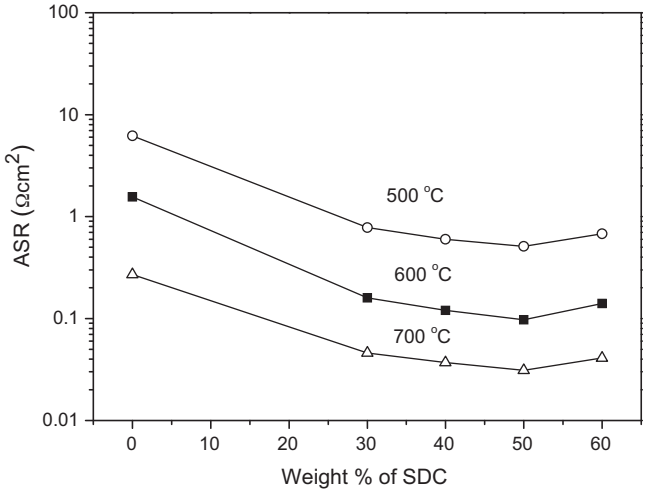

Fig. 4. ASR results as a function of weight percentage of SDC in the PNC–SDC composite cathode at several fixed temperatures.

from 0.27 Ω cm^2 for the pure PNC to 0.046 Ω cm^2 when 30% SDC was added. This value decreases further to 0.031 Ω cm^2 when 50% SDC was added, which is only 11.5% of the original value. This might be due to the fact that the addition of SDC results in improving the oxygen ion diffusion, increasing the triple phase boundaries where the oxygen reduction reaction occurs, and meanwhile enhancing the bonding between the electrolyte and electrode. As the SDC content increases, the SDC particles gradually form a continuous network in the PNC matrix, extending the TPBs from the physical cathode/electrolyte interface to the bulk of cathode.

The ASR value of the PNC–SDC composite cathode is found to be not only much lower (4–10 times) than that of the pure PNC cathode, but also significantly lower than those of LSCF–SDC, LNC–SDC, as well as other cobalt-containing cathodes like $Sm_{0.5}Sr_{0.5}CoO_3$–SDC and so on [6,8,15]. The low polarization resistances are also comparable to those of $Ba_{0.5}Sr_{0.5}Co_{0.8}Fe_{0.2}O_3$–SDC, $SmBa_{0.5}Sr_{0.5}Co_2O_6$–SDC cathodes, indicating the present cathode is more suitable for SOFC cathode material [10,13].

For the pure PNC, the apparent activation energy was 1.31 eV, and for the PNC–SDC composite cathodes, the apparent activation energy was found to vary from 1.19 eV to 1.24 eV. SDC addition has no obvious influence on the apparent activation energy, suggesting that the introducing of SDC into the PNC cathode does not significantly affect the mechanism of oxygen reduction.

The comparison shows that the lowest polarization resistance was obtained at the ratio of PNC:SDC to be 50:50. This agrees well with the effective medium percolation theory of composite cathodes, which predicates the maximum triple phase boundary for electrochemical exchange at that ratio. However, this advantage can only be realized once the secondary phase has formed percolating network, allowing the full extent of the increased triple phase boundary to be utilized.

Fig. 4 shows the ASR as a function of SDC content at several fixed temperatures. It is clearly seen that, with increasing SDC content, the ASR value decreases initially, passes though a minimum at SDC content around 50%, and then increases for further addition of SDC. This feature agrees very well with the percolation model as aforementioned. Below the percolation limit (SDC content <50%), the addition of the SDC merely disrupts the conduction in the electrode, leading to higher observed resistance; as it reaches the percolation threshold, the full triple-phase-boundary network is able to contribute to the electrochemical processes, resulting in a reduced polarization. As the SDC level continues to increase, the polarization resistance increases again as the percolation in the PNC phase will be destroyed by the high levels of SDC. One, thus, would expect a minimum ASR in the mixture with a ratio of 50:50 of the two phases, where the best balance between the maximum triple phase boundary and the percolation in both phases is achieved.

Fig. 5a shows the measured impedance spectra at 700 °C for the PNC and PNC–50SDC cathodes. The difference between the high frequency and low frequency intercepting with the real axis represents the area specific resistance (ASR) of the cathode. The impedance of a cathode actually is the sum of charge-transfer resistance, impedance, and a "chemical" impedance associated with non-charge-transfer processes [24,25]. The contribution at intermediate/high frequencies is related essentially to electron and ion transfer at the electrode/electrolyte interfaces; while the contribution at low frequencies can be associated with non-charge-transfer processes (including oxygen surface exchange, solid-state diffusion, and gas-phase diffusion inside and outside the electrode). In most cases, the impedance spectrum consists of multiple

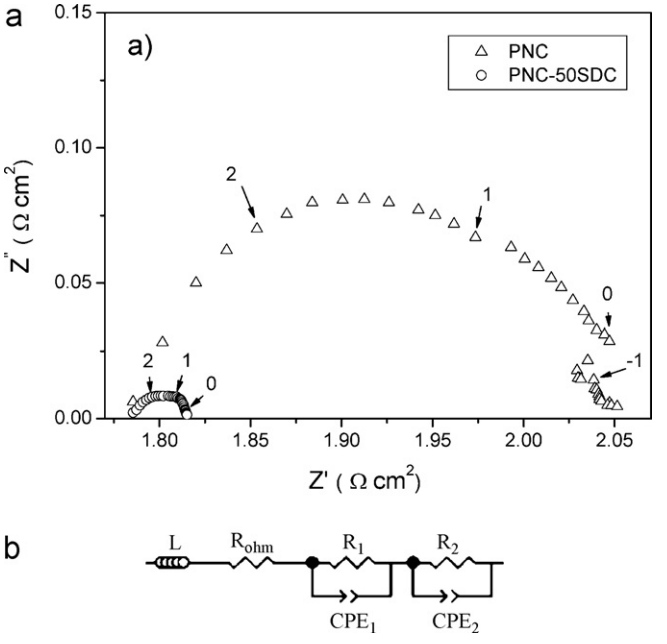

Fig. 5. AC impedance spectra of PNC and PNC–50SDC cathodes at 700 °C in air (a) and the corresponding equivalent circuit (b). The numbers in the plots correspond to logarithm of frequency.

semi-circles, indicating different electrode reaction processes occurring at different time scales and contributing significantly to the total electrode polarization resistance [25–28]. The impedance spectra of the pure PNC and PNC–50SDC electrodes exhibit two arcs in their spectra at 700 °C.

For comparative analysis of the single phase and composite cathodes, the cathode polarization was analyzed by fitting the impedance spectra to an equivalent circuit (EQC) shown in Fig. 5b. The equivalent circuit comprises of an inductor, series resistance and two distributed elements each consisting of a resistor and constant phase element (CPE) in parallel with the distributed elements representing the middle and low frequency arcs. In the equivalent circuit, the resistance from the middle-frequency arc is attributed to the charge transfer (*R1*), and the lower-frequency arc to the oxygen dissociation and bulk or surface oxygen diffusion process (*R*2). One can see from Fig. 5a that the *R*2 values are higher than those of *R*1 in the PNC cathode system. This implies that the cathodic polarization of the composite cathode is governed by *R*2 at 700 °C. However, *R*1 is higher than *R*2 in the PNC–50SDC cathode, suggesting that charge-transfer resistance can be considered as the rate-determining step in the single-phase cathode at 700 °C.

The performance of the PNC and PNC–50SDC cathode was further evaluated using a single cell based on a SDC electrolyte and Ni–SDC anode with an YSZ buffer interlayer. Fig. 6 shows the cell voltage and power density as a function of current density for cells with the PNC and PNC–50SDC cathodes at 700 °C. With humidified (3% H_2O) hydrogen as the fuel and ambient air as the oxidant, the maximum power densities of the cell with the PNC and PNC–50SDC

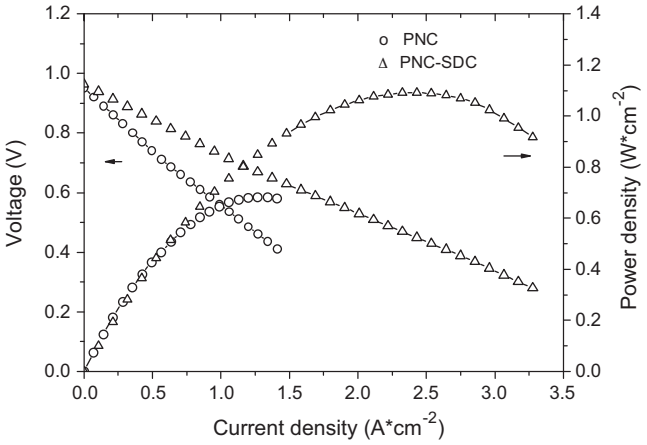

Fig. 6. I–V performance measured at 700 °C for Ni–SDC supported thin SDC electrolyte with PNC and PNC–50SDC cathodes.

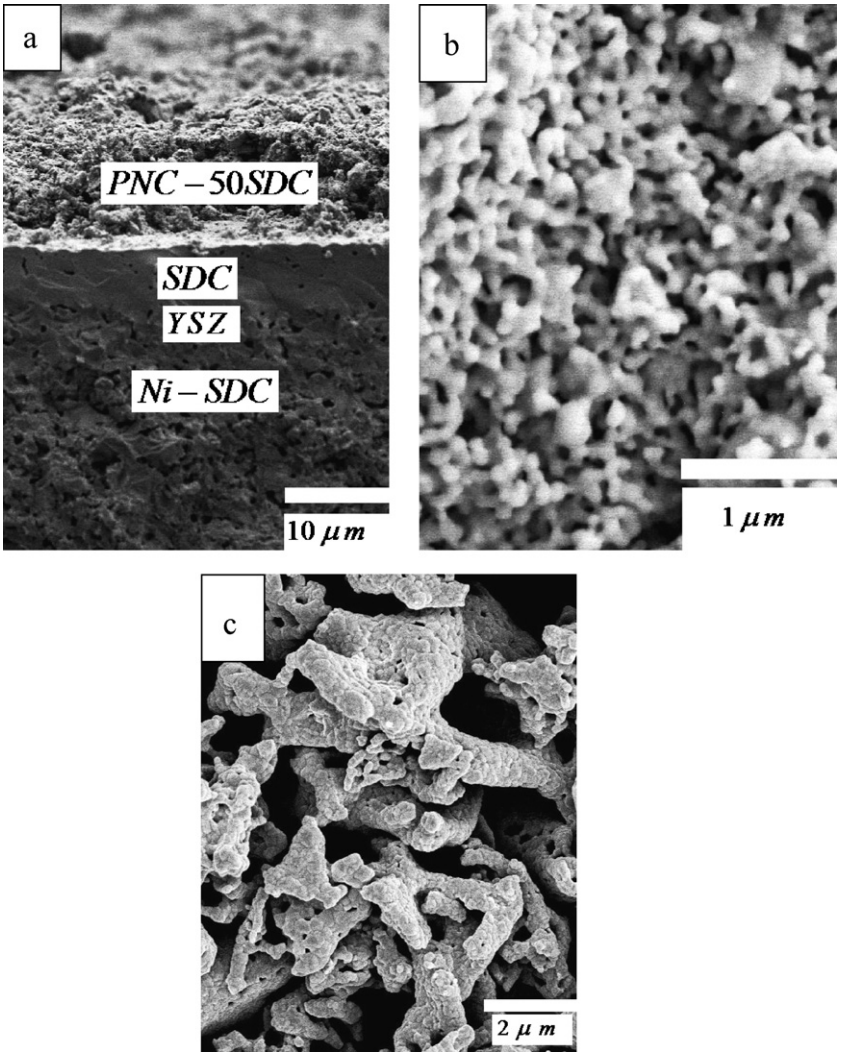

Fig. 7. SEM images of (a) the cross-sectional microstructures of PNC–50SDC, (b) the surface microstructures of the PNC–SDC cathodes sintered at 950 °C for 2 h, and (c) the microstructures of the PNC powders fired at 900 °C for 2 h.

Table 1
Thermal expansion coefficient of PNC and PNC–50SDC at different temperatures.

Sample	TEC ($\times 10^{-6}$ K^{-1})				
	25–600 °C	25–700 °C	25–800 °C	25–900 °C	25–1000 °C
PNC	13.64	14.21	14.86	15.62	16.23
PNC–50 SDC	13.16	13.49	13.87	14.26	14.52

cathodes are found to be 586 and 1090 mWcm^{-2} with the open circuit voltage (OCV) of 0.92 V and 0.93 V, respectively. Considering the electronic conductivity of SDC which causes short circuit in the cell, the OCV hints that the electrolyte membrane is sufficiently dense, which is in good agreement with the result of SEM observation shown in the next figure. The cell performance suggests that the PNC–50SDC is a very promising cathode material for ITSOFCs.

Fig. 7a presents the cross-sectional image of the as-prepared cell. As can be seen from Fig. 7a, the well-sintered SDC electrolyte membrane is quite dense with a thickness of about 10 μm. It is clear that the PNC–50SDC cathode layer contains large number of porosity, which is favorable for the diffusion and activation of the O_2 molecules, and adheres well to the electrolyte. The cathodes display a fine uniform microstructure with appropriate porosity. There are no delamination and crack in the interfaces, suggesting a good thermal compatibility between the two materials. Shown in Fig. 7b and c are the typical surface SEM image of the PNC–50SDC cathode sintered at 950 °C for 2 h and the SEM image of PNC powder fired at 900 °C for 2 h. The microstructure shows that the cathode contains regular-shaped particles with about 0.1–0.2 μm in size (Fig. 7b). The particles connect with each other forming a porously continuous network structure.

The good thermal compatibility between the PNC–50SDC cathode and SDC electrolyte could be partly explained based on the results of their thermal expansion coefficients (shown in Table 1). Thermal expansion curves with increasing temperature for the PNC and PNC–50SDC cathodes are given in Fig. 8.

The TEC value of the PNC is close to that of the LNC (about 14–15 $\times 10^{-6}$ K^{-1}), and lower than that of the LSCF (17.5 $\times 10^{-6}$ K^{-1}). Moreover, the addition of 50 wt.% SDC into PNC can further decrease the TEC. The TEC of the PNC–SDC is 13.49 $\times 10^{-6}$ K^{-1} at 700 °C, which is very close to that of the SDC electrolyte (12.8 $\times 10^{-6}$ K^{-1}), and thus the effective expansion of the PNC–50SDC composite cathode will be matched relatively well with the rest of the cell. This good chemical and thermal compatibility might be favorable for the cell long-term stability.

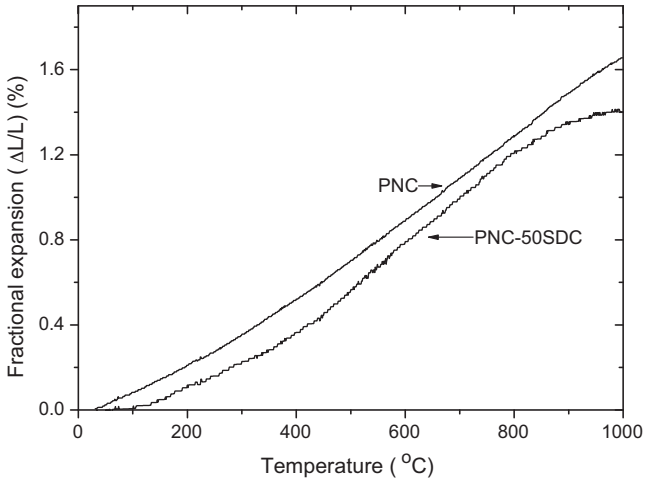

Fig. 8. Fractional thermal expansion of PNC and PNC–50 wt.% SDC in air.

4. Conclusions

$PrNi_{0.6}Co_{0.4}O_3$–$Ce_{0.8}Sm_{0.2}O_{1.9}$ has been evaluated as new composite cathodes for intermediate temperature solid oxide fuel cells. Single-phase perovskite PNC exhibited metallic behavior with electrical conductivities of 1580 S cm^{-1} at 50 °C and 1031 S cm^{-1} at 1000 °C. The area specific resistances of the PNC and PNC–50SDC cathodes on the SDC electrolyte were as low as 0.27 Ω cm^2 and 0.031 Ω cm^2 at 700 °C, respectively. A maximum power density of a single cell was found to be 1090 mW cm^{-2} at 700 °C with a cell of a 10 μm thick SDC electrolyte and a PNC–50SDC cathode. The TEC of the PNC–50SDC composite cathode is 13.49 $\times 10^{-6}$ K^{-1} at 700 °C. The PNC–50SDC cathode is chemical and thermal compatibility with the SDC electrolyte. Our preliminary results suggest that PNC–50SDC is a very promising cathode for ITSOFCs.

Acknowledgments

The authors gratefully thank the financial support from Anhui Key Laboratory of Information Materials and Devices and National Natural Science Foundation of China (Grant No. 11074001).

References

[1] N.Q. Minh, J. Am. Ceram. Soc. 76 (1993) 563–588.
[2] B.C.H. Steele, A. Heinzel, Nature 414 (2001) 45–352.
[3] N.P. Brandon, S. Skinner, B.C.H. Steele, Annu. Rev. Mater. Res. 33 (2003) 183–213.
[4] S.J. Skinner, Int. J. Inorg. Mater. 3 (2001) 113–121.
[5] H. Uchida, S. Arisaka, M. Watanabe, Solid State Ionics 135 (2000) 347–351.
[6] E.P. Murray, M.J. Sever, S.A. Barnett, Solid State Ionics 148 (2002) 7–34.
[7] S.P. Jiang, Solid State Ionics 146 (2002) 1–22.
[8] C.R. Xia, W. Rauch, F.L. Chen, M.L. Liu, Solid State Ionics 149 (2002) 11–19.
[9] A. Esquirol, N.P. Brandon, J.A. Kilner, M. Mogensen, J. Electrochem. Soc. 151 (2004) A1847–A1855.
[10] Z.P. Shao, S.M. Haile, Nature 431 (2004) 170–173.
[11] A. Chang, S.J. Skinner, J.A. Kilner, Solid State Ionics 177 (2006) 2009–2011.
[12] J.H. Kim, J. Bae, M. Cassidy, P.A. Connor, W. Zhou, J.T.S. Irvine, ECS Trans. 25 (2009) 2707–2715.
[13] J.H. Kim, M. Cassidy, J.T.S. Irvine, J. Bae, Chem. Mater. 22 (2010) 883–892.
[14] M.C. Tucker, L. Cheng, L.C. DeJonhe, J. Power Sources 196 (2011) 8313–8322.
[15] P. Hjalmarsson, M. Mogensen, J. Power Sources 196 (2011) 7237–7244.
[16] Y.P. Fu, Int. J. Hydrogen Energy 36 (2011) 5574–5580.
[17] J. Molenda, K. Świerczek, W. Zając, J. Power Sources 173 (2007) 675–680.
[18] P. Hjalmarsson, M. Søgaard, M. Mogensen, J. Solid State Chem. 183 (2010) 1853–1862.
[19] H. Taguchi, R. Takeshi Komatsu, K. Chiba, H. Nozawa, H. Orui, Arai, Solid State Ionics 182 (2011) 127–132.
[20] R.R. Peng, C.R. Xia, Q.X. Fu, G.Y. Meng, D.K. Peng, Mater Lett. 56 (2002) 1043–1047.
[21] S.W. Zha, C.R. Xia, G.Y. Meng, J. Power Sources 115 (2003) 44–48.
[22] X.G. Zhang, M. Robertson, C.D. Petit, W. Qu, O. Kesler, R. Maric, D. Ghosh, J. Power Sources 164 (2007) 668–677.
[23] H. Moon, S.D. Kim, S.H. Hyun, H.S. Kim, Int. J. Hydrogen Energy 33 (2008) 2826–2833.
[24] S.B. Adler, Solid State Ionics 111 (1998) 125–134.
[25] S.B. Adler, Solid State Ionics 135 (2000) 603–612.
[26] Z.Y. Jiang, L. Zhang, L.L. Cai, C.R. Xia, Electrochim. Acta 54 (2009) 3059–3965.
[27] A. Barbucci, M. Viviani, M. Panizza, M. Delucchi, G. Cerisola, J. Appl. Electrochem. 35 (2005) 399–403.
[28] K. Huang, H.Y. Lee, J.B. Goodenough, J. Electrochem. Soc. 145 (1998) 3220–3227.